PREDICTING THE RESIDUAL STIFFNESS PROPERTIES OF CARBON FIBRE/EPOXY LAMINATES LOADED IN THERMAL FATIGUE

Costas Soutis and Maria Kashtalyan
Aerospace Engineering, The University of Sheffield, Mappin Street,
Sheffield S1 3JD, UK. c.soutis@sheffield.ac.uk

ABSTRACT

The failure process in composite layered plates under quasi-static or fatigue tensile or thermal loading involves sequential accumulation of damage in the form of matrix cracking in the off-axis plies of the laminate, matrix crack-induced local and edge delaminations, fiber-matrix debonding and fiber breakage. Accurate prediction of the laminate strength and stiffness response to damage must consider the above-mentioned damage mechanisms. In this paper, an approach is presented for the analysis of cross-ply laminates, damaged at microscopic level by transverse and longitudinal matrix cracks accompanied by transverse and longitudinal delaminations along them. The model is based on the Equivalent Constraint Model (ECM) of the damaged ply and employs an improved 2-D shear lag method to determine the stress field in the damaged ply (of thickness 125 μm). The approach is applied to predict stiffness reduction in T300/914 carbon fibre/epoxy cross-ply laminates using experimentally observed damage patterns under thermal fatigue loading.

1. INTRODUCTION

Resin-dominated damage modes such as matrix cracking and delamination are common failure mechanisms in composite laminates and are of primary concern in the current design with composites. Matrix cracking in the 90^o ply has long been recognised as the first damage mode observed under static and fatigue tensile or thermal loading. In cross-ply laminates matrix cracks may appear both in the 90^o and 0^o plies and be accompanied by local delaminations growing along the cracks at the $0^o/90^o$ interface.
Damage mechanisms and damage accumulation in cross-ply composite laminates under quasi-static and fatigue loading have been the subject of many investigations, e.g. [1-8]. However, multilayer damage of cross-ply laminates has been very little modelled theoretically or simulated numerically (by means of finite elements), mainly because the analysis of a representative segment defined by intersecting pairs of cracks is very cumbersome. Hashin [9], Tsai and Daniel [10], Henaff-Gardin et al [11] developed analytical models to predict residual stiffness of cross-ply laminates damaged by transverse and longitudinal matrix cracking. The residual stiffness is representative of the damage state within the specimen and can be measured frequently during damage development. It is a potential non-destructive test parameter, which can be used to monitor damage in a structural component. However, none of the models [9-11] takes into consideration local delaminations developing between the plies along transverse and longitudinal matrix cracks.

In this paper, an approach is presented that has been developed to predict residual stiffness (macroscopic response) of cross-ply laminates damaged at microscopic level by transverse and longitudinal matrix cracks accompanied by local delaminations along them. It is based on the Equivalent Constrain Models (ECM) of the damaged ply and employs an improved 2-D shear lag method to determine stresses in the damaged ply. The approach is then used to predict the residual stiffness of T300/914 cross-ply laminates with damage patterns, experimentally observed under thermal fatigue loading.

2. DAMAGE CHARACTERISATION

Figure 1 shows a cross-ply $[0_m/90_n]_s$ laminate subjected to biaxial tension ($\overline{\sigma}_{11}$ and $\overline{\sigma}_{22}$) and shear loading ($\overline{\sigma}_{12}$). Suppose transverse and longitudinal matrix cracks are spaced uniformly and span the full thickness and width of the 90^o and 0^o plies respectively, and strip-shaped transverse and longitudinal delaminations grow along respective sets of cracks at the $0^o/90^o$ interface. Let $2s_1$ and $2s_2$ denote the spacing between longitudinal and transverse cracks, and $2\ell_1$ and $2\ell_2$ denote the width of longitudinal and transverse delamination strips, respectively.

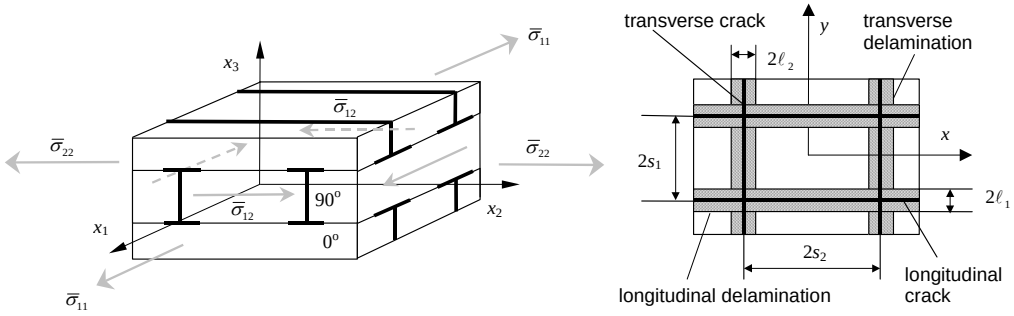

a) b)

Figure 1. Damaged cross-ply laminate under general in-plane loading: a) general view; b) plan view.

2.1 Equivalent Constraint Model (ECM)

To analyse cracks associated with delaminations, it was suggested [12] to consider the following two ECM laminates instead of a representative segment the damaged laminate defined by intersecting pairs of cracks. In the ECM1 laminate, the 0^o layer (1^{st} layer) contains damage explicitly, while the 90^o layer (2^{nd} layer), damaged by transverse cracking and transverse delaminations, is replaced with a homogeneous equivalent constraint one with reduced stiffness properties. Likewise, in the ECM2 laminate, the 90^o layer (2^{nd} layer) is damaged explicitly, while the 0^o layer (1^{st} layer), damaged by longitudinal matrix cracks and longitudinal delaminations, is replaced with the homogeneous equivalent constraint one with reduced stiffness properties.

The purpose of the analysis of the ECM1 laminate is to determine the stress field in its explicitly damaged 1st layer and the reduced stiffness properties of the homogeneous layer, equivalent to it. It is assumed that the stiffness properties of the equivalent constraint 2nd layer, used in the analysis of the ECM1 laminate, are known from the analysis of the ECM2 laminate. This makes problems for ECM1 and ECM2 laminates entwined.

3. STRESS ANALYSIS

ECM1 and ECM2 laminates are referred to the co-ordinate system $x_1x_2x_3$ (Fig. 1). Representative segment of an ECMμ laminate, containing either a pair of cracks ($\mu=1$) or a single crack ($\mu=2$) and two crack tip delaminations, can be segregated into the locally delaminated ($0<|x_\mu|<\ell_\mu$) and perfectly bonded ($\ell_\mu<|x_\mu|<s_\mu$) regions. Due to symmetry, the analysis can be restricted to one quarter of the segment (Fig. 2).

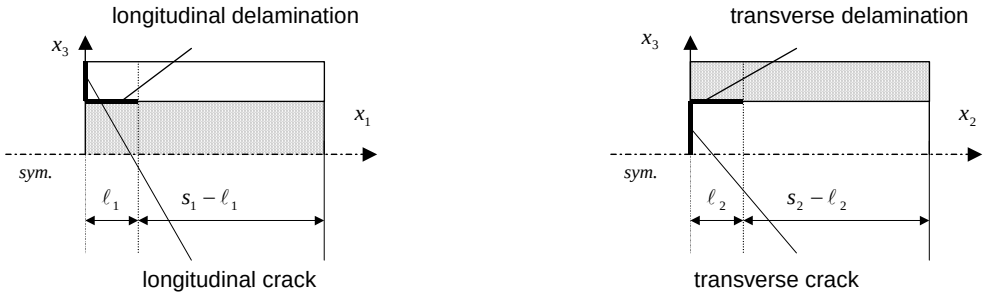

a) b)

Figure 2. Representative through-thickness segments of: a) ECM1 laminate; b) ECM2 laminate

Since crack and delamination surfaces are assumed stress-free, stresses in the locally delaminated region of the explicitly damaged μ^{th} ply vanish. In the perfectly bonded region, the in-plane microstresses $\sigma_{j\mu}^{(\mu,\mu)}$, $j=1,2$ can be determined from the equilibrium equations

$$\frac{d}{dx_\mu}\tilde{\sigma}_{j\mu}^{(\mu,\mu)}+(-1)^\mu\frac{\tau_j^{(\mu)}}{h_\mu}=0,\quad j,\mu=1,2 \tag{1}$$

The out-of-plane shear stresses are assumed to vary linearly across the thickness of the 90^o layer as well as over one-single-ply thickness in the 0^o layer (so called shear layer) [13]. By integrating the constitutive equations for the out-of-plane shear stresses (see Appendix A of [14]), the interface shear stresses $\tau_j^{(\mu)}$ are expressed as

$$\tau_j^{(\mu)}=K_j(\tilde{u}_j^{(\mu,1)}-\tilde{u}_j^{(\mu,2)}),\quad K_j=\frac{3\hat{G}_{j3}^{(1)}\hat{G}_{j3}^{(2)}}{h_2\hat{G}_{j3}^{(1)}+(1+(1-\eta)/2)\eta h_1\hat{G}_{j3}^{(2)}},\quad \eta=t/h_1 \tag{2}$$

Substitution of shear lag equations, Eqs. (2), into equilibrium equations, Eqs. (1) and subsequent differentiation with respect to x_μ yield

$$\frac{d^2}{dx_\mu^2}\widetilde{\sigma}_{\mu\mu}^{(\mu,\mu)} + (-1)^\mu \frac{K_j}{h_\mu}(\widetilde{\varepsilon}_{\mu\mu}^{(\mu,1)} - \widetilde{\varepsilon}_{\mu\mu}^{(\mu,2)}) = 0, \quad \frac{d^2}{dx_\mu^2}\widetilde{\sigma}_{12}^{(\mu,\mu)} + (-1)^\mu \frac{K_j}{h_\mu}(\widetilde{\gamma}_{12}^{(\mu,1)} - \widetilde{\gamma}_{12}^{(\mu,2)}) = 0 \tag{3}$$

Strain differences $(\widetilde{\varepsilon}_{\mu\mu}^{(\mu,1)} - \widetilde{\varepsilon}_{\mu\mu}^{(\mu,2)})$ and $(\widetilde{\gamma}_{12}^{(\mu,1)} - \widetilde{\gamma}_{12}^{(\mu,2)})$ can be expressed in terms of stresses $\widetilde{\sigma}_{\mu\mu}^{(\mu,\mu)}$ and $\widetilde{\sigma}_{12}^{(\mu,\mu)}$, using the equations of the global equilibrium of the laminate, constitutive equations for both layers, as well as the condition of generalised plane strain in the plane $Ox_\mu x_3$. Finally, Eqs. (3) are reduced to two second-order ordinary differential equations with the following solutions

$$\widetilde{\sigma}_{\mu\mu}^{(\mu,\mu)} = \frac{1}{L_1^{(\mu)}} f_1(\chi_\mu, s_\mu, \ell_\mu)(\mathbf{\Omega}_{11}^{(\mu)}\overline{\sigma}_{11} + \mathbf{\Omega}_{22}^{(\mu)}\overline{\sigma}_{22}), \quad \widetilde{\sigma}_{12}^{(\mu,\mu)} = \frac{1}{L_2^{(\mu)}} f_2(\chi_\mu, s_\mu, \ell_\mu)\mathbf{\Omega}_{12}^{(\mu)}\overline{\sigma}_{12}, \tag{4}$$

$$f_j(\chi_\mu, s_\mu, \ell_\mu) = 1 - \cosh[\sqrt{L_j^{(\mu)}}(x_\mu - s_\mu)]\cosh^{-1}[\sqrt{L_j^{(\mu)}}(s_\mu - \ell_\mu], \quad j = 1,2$$

Constants $L_1^{(\mu)}, L_1^{(\mu)}, \mathbf{\Omega}_{11}^{(\mu)}, \mathbf{\Omega}_{22}^{(\mu)}, \mathbf{\Omega}_{12}^{(\mu)}$ depend on the stiffnesses $\hat{Q}_{ij}^{(\mu)}$ of the intact material of the μ^{th} layer, modified (due to the implicitly contained damage) stiffnesses $Q_{ij}^{(\kappa)}, \kappa \neq \mu$ of the equivalent constraint layer, shear lag parameters K_j and the layer thickness ratio χ. In detail, they are presented in [14].

4. STIFFNESS ANALYSIS

In order to determine the reduced stiffness properties of the damaged laminate, the reduced stiffness properties of the homogeneous layer, equivalent to the explicitly damaged ply, need to be determined first. Constitutive equations of the equivalent homogeneous layer have the form

$$\{\overline{\sigma}^{(\mu,\mu)}\} = [Q^{(\mu)}]\{\overline{\varepsilon}^{(\mu,\mu)}\} \tag{5}$$

The in-plane stiffness matrix $[Q^{(\mu)}]$ of the homogeneous layer, equivalent to the explicitly damaged μ^{th} ply, is related to the in-plane stiffness matrix $[\hat{Q}^{(\mu)}]$ of the pristine material via In-situ Damage Effective Functions (IDEFs) $\mathbf{\Lambda}_{22}^{(\mu)}$, $\mathbf{\Lambda}_{66}^{(\mu)}$ as

$$[Q^{(\mu)}] = [\hat{Q}^{(\mu)}] - [\hat{R}^{(\mu)}][\mathbf{\Lambda}^{(\mu)}] \tag{6}$$

$$[\hat{R}^{(\mu)}]=\begin{bmatrix}\hat{R}_{11}^{(\mu)} & \hat{Q}_{12}^{(\mu)} & 0\\ \hat{Q}_{12}^{(\mu)} & \hat{R}_{22}^{(\mu)} & 0\\ 0 & 0 & \hat{Q}_{66}^{(\mu)}\end{bmatrix},\quad [\boldsymbol{\Lambda}^{(\mu)}]=\begin{bmatrix}\boldsymbol{\Lambda}_{22}^{(\mu)} & 0 & 0\\ 0 & \boldsymbol{\Lambda}_{22}^{(\mu)} & 0\\ 0 & 0 & \boldsymbol{\Lambda}_{66}^{(\mu)}\end{bmatrix}$$

$$\hat{R}_{\mu\mu}^{(\mu)}=\hat{Q}_{\mu\mu}^{(\mu)},\quad \hat{R}_{22}^{(1)}=(\hat{Q}_{12}^{(1)})^2(\hat{Q}_{11}^{(1)})^{-1},\quad \hat{R}_{11}^{(2)}=(\hat{Q}_{12}^{(2)})^2(\hat{Q}_{22}^{(2)})^{-1} \tag{6}$$

The lamina macrostresses $\{\overline{\sigma}^{(\mu,\mu)}\}$ in the equivalent ply can be obtained by averaging the in-plane microstresses, Eq. (4), across the length of the representative segment as

$$\overline{\sigma}_{\mu\mu}^{(\mu,\mu)}=\frac{1}{L_1^{(\mu)}}(1-\tanh[\sqrt{L_1^{(\mu)}}(s_\mu-\ell_\mu)])(\boldsymbol{\Omega}_{11}^{(\mu)}\overline{\sigma}_{11}+\boldsymbol{\Omega}_{22}^{(\mu)}\overline{\sigma}_{22}) \tag{7a}$$

$$\overline{\sigma}_{12}^{(\mu,\mu)}=\frac{1}{L_2^{(\mu)}}(1-\tanh[\sqrt{L_2^{(\mu)}}(s_\mu-\ell_\mu)])\boldsymbol{\Omega}_{12}^{(\mu)}\overline{\sigma}_{12} \tag{7b}$$

The lamina macrostrains $\{\overline{\varepsilon}^{(\mu,\mu)}\}$ are assumed to be equal to those in the equivalent constraint ply, i.e. $\{\overline{\varepsilon}^{(\mu,\mu)}\}=\{\overline{\varepsilon}^{(\mu,\kappa)}\}$, as well as to the applied laminate strain, and are calculated from the constitutive equations for the equivalent constraint ply and the laminate equilibrium equations.

Substitution of Eq. (6) into constitutive equations, Eq. (5), for the equivalent homogeneous layer yields IDEFs in terms of the lamina macrostresses and lamina macrostrains as

$$\boldsymbol{\Lambda}_{22}^{(1)}=1-\frac{\overline{\sigma}_{11}^{(1,1)}}{\hat{Q}_{11}^{(1)}\overline{\varepsilon}_{11}^{(1,1)}+\hat{Q}_{12}^{(1)}\overline{\varepsilon}_{21}^{(1,1)}},\quad \boldsymbol{\Lambda}_{22}^{(2)}=1-\frac{\overline{\sigma}_{22}^{(2,2)}}{\hat{Q}_{12}^{(2)}\overline{\varepsilon}_{11}^{(2,2)}+\hat{Q}_{22}^{(2)}\overline{\varepsilon}_{22}^{(2,2)}},$$
$$\boldsymbol{\Lambda}_{66}^{(\mu)}=1-\frac{\overline{\sigma}_{12}^{(\mu,\mu)}}{\hat{Q}_{66}^{(\mu)}\overline{\gamma}_{12}^{(\mu,\mu)}} \tag{8}$$

Finally, closed-form expressions for IDEFs are obtained

$$\boldsymbol{\Lambda}_{qq}^{(\mu)}=1-\frac{1-\boldsymbol{\Phi}_q(D_\mu^{mc},D_\mu^{ld})}{\dfrac{1+\beta_q^{(\mu)}D_\mu^{ld}}{1-D_\mu^{ld}}+\gamma_q^{(\mu)}\boldsymbol{\Phi}_q(D_\mu^{mc},D_\mu^{ld})},$$

$$\boldsymbol{\Phi}_q(D_\mu^{mc},D_\mu^{ld})=\frac{D_\mu^{mc}}{\beta_q^{(\mu)}(1-D_\mu^{ld})}\tanh\left[\frac{\beta_q^{(\mu)}(1-D_\mu^{ld})}{D_\mu^{mc}}\right],\ q=2,6 \tag{9}$$

Constants $\beta_q^{(\mu)},\gamma_q^{(\mu)}, q=2,6, \mu=1,2$ depend solely on the initial stiffnesses $\hat{Q}_{ij}^{(\mu)}$ of the μ^{th} layer, modified stiffnesses $Q_{ij}^{(\kappa)}, \kappa\neq\mu$ of the equivalent constraint κ^{th} layer, shear

lag parameters K_j as well as the layer thickness ratio and are given in detail in [14]. The modified stiffnesses $Q_{ij}^{(\kappa)}$ of the equivalently constraining κ^{th} layer are determined from the analysis of the ECMκ laminate and are functions of the IDEFs $\Lambda_{22}^{(\kappa)}, \Lambda_{66}^{(\kappa)}$, depending explicitly on the damage parameters $D_\kappa^{mc} = h_\kappa / s_\kappa, D_\kappa^{ld} = \ell_\kappa / s_\kappa$. Therefore, the IDEFs for both layers depend on each other. They form a system of four simultaneous nonlinear algebraic equations, which is solved computationally by a direct iterative procedure.

5. RESULTS AND DISCUSSION

In absence of delaminations, the developed ECM/2-D shear lag approach has been validated by comparing its predictions with those obtained from the earlier developed models [9-11]. The results of comparison are published elsewhere [15].

Figure 3 shows observed damage development and predicted stiffness reduction in a cross-ply $[0_4/90_4]_s$ T300/914 carbon epoxy laminate during thermal cycling.

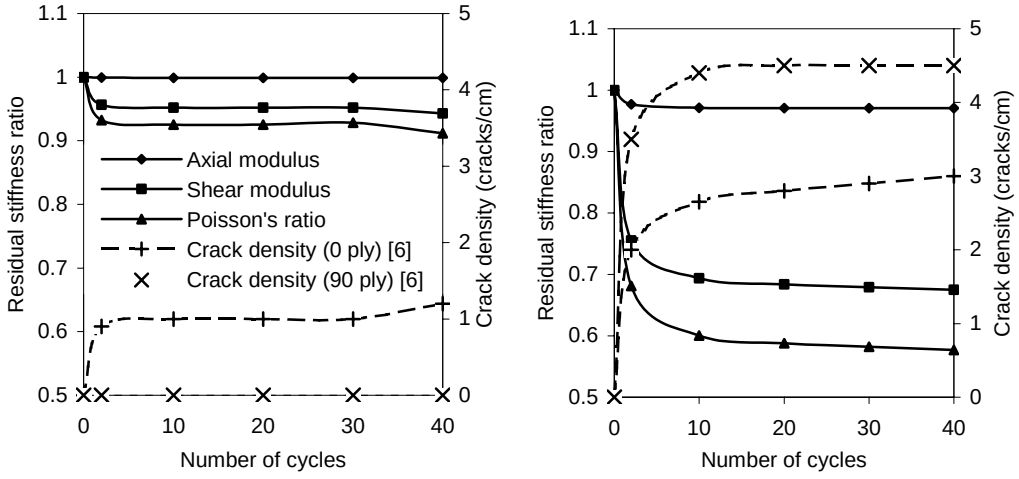

Figure 3. Stiffness reduction and damage development for a T300/914 $[0_4/90_4]_s$ laminate under thermal cycling: a) –200°C/ +20°C; b)–200°C/ +90°C

Each cycle consisted of cooling at –200°C and heating at +20°C or +90°C, and crack density in the 90° and 0° plies was measured [7]. However the size of growing delaminations that accompanied longitudinal cracks in the –200° C/+90°C cycling was not. Predictions of reduction in the axial and shear moduli as well as the Poisson's ratio are shown along with the measured crack densities as a function of the number of cycles. During the $-200°C/+20°C$ cycling, (Fig. 3a), the predicted stiffness reduction is less than 10% for all stiffness properties due to zero crack density in the 90° ply. As transverse cracks developed during the $-200°C/+90°C$ cycling, the shear modulus and Poisson's ratio underwent up to 40% reduction. However, the predicted reduction of the axial stiffness in this case is less than 5%, Fig. 3b. This indicates that the shear modulus

and the Poisson's ratio could be much better parameters to characterise stiffness degradation of the laminate than the axial modulus.

Since the size of the delamination area was not measured during cycling, reduction of stiffness properties of $[0_4/90_4]_s$ T300/914 laminate due to delaminations was predicted using assumed delamination sizes. Strip-width of the transverse delamination was set to zero, while that of the longitudinal delamination allowed variation from zero to 50%. In other words, longitudinal delaminations were assumed to have propagated from the crack tip to one quarter of the distance between two cracks. This seems to be a reasonable assumption, consistent with X-ray radiographs obtained in [7]. In Fig. 4, predicted reductions of the axial, transverse and shear moduli as well as Poisson's ratio are plotted as function of the relative delamination area.

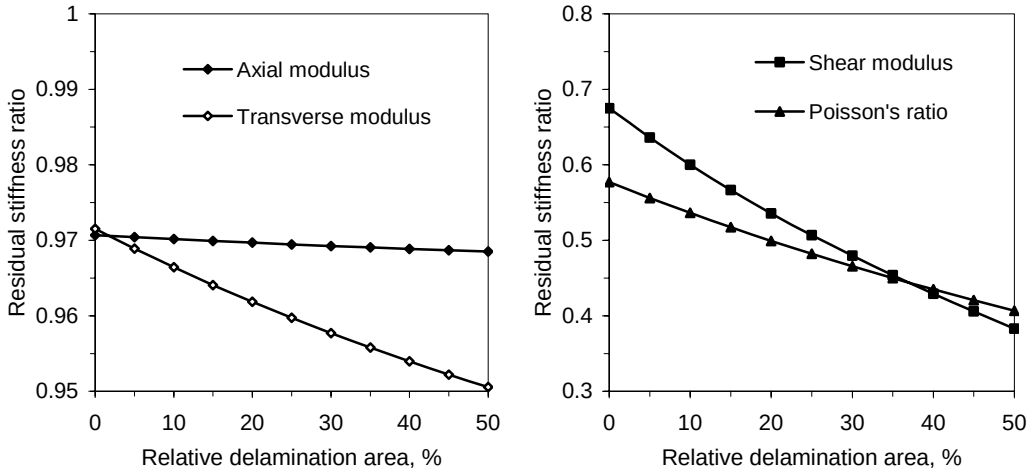

a) b)

Figure 4. Stiffness reduction of a T300/914 $[0_4/90_4]_s$ laminate as a function of the relative longitudinal delamination area after approximately 20 cycles at –200°C/ +90°C: a) axial and transverse moduli; b) shear modulus and Poisson's ratio. Crack densities (saturated values) in the 0° ply $C_1 = 3\,\text{crack/cm}$ and in the 90° ply $C_2 = 4.5\,\text{crack/cm}$.

The axial modulus appear to be unaffected by the growth of delamination, while transverse modulus is further reduced, but not significantly, Fig. 4a. The reduction in the shear modulus is more pronounced than in the Poisson's ratio, Fig. 4b. Crack densities in 90° and 0° plies were taken as C_2=4.5 cracks/cm and C_1=3 cracks/cm respectively, which corresponds to saturation values reached during the –200°C/+90°C cycling. Under uniaxial tensile loading, longitudinal delaminations appear to be more important than the transverse one, since they result in isolation of the portions of the load-bearing 0° plies, which become prone to fibre breakage. Under biaxial tensile loading, the importance of one set of delaminations over the other depends very much on the biaxiality and ply thickness ratios. Recent work has extended the model to off-axis dominated laminates $[\pm\theta/0]_{ns}$ where matrix cracking and local delamination appear in the θ ply [16-17]. In practical applications the type of damage analysed in this paper

can be detected non-destructively by employing structural health monitoring methods based for instance on Lamb waves generated by piezoelectric transducers [18-20] or embedded shape memory alloy wires [21].

6. ACKNOWLEDGEMENTS

Financial support of this research by the Engineering and Physical Sciences Research Council (EPSRC/GR/L51348) and Ministry of Defence, UK, is gratefully acknowledged.

7. REFERENCES

1. Parvizi, A., Garret, K.W., and Bailey, J.E., *J. Mat. Sci.*, **13**, 1978, 195-201
2. Daniel, I.M., and Charewicz, A., *Eng. Fracture Mechanics*, **25**(5-6), 1986, 793-808
3. Jamison, R.D., Schulte, K., Reifsnider, K.L., and Stinchcomb, W.W., Characterization and Analysis of Damage Mechanisms in Tension-Tension Fatigue of Graphite/Epoxy Laminates, *Effects of Defects in Composite Materials, ASTM STP 836*, American Society for Testing and Materials, Philadelphia, 1984, 21-55
4. Smith, P.A., Wood, J.R., *Composites Science and Technology*, **38**(1), 1990, 85-93
5. Charewicz, A., and Daniel, I.M., Damage Mechanisms and Accumulation in Graphite/Epoxy Laminates, *Composite Materials: Fatigue and Fracture, ASTM STP 907*. H.T. Hahn, Ed., American Society for Testing and Materials, Philadelphia, 1986, 274-297
6. Boniface, L., and Ogin, S.L., *J. Comp. Materials*, **23**, 1989, 735-754
7. Henaff-Gardin, C., Lafarie-Frenot, M.C., and Gamby, D., *Comp. Structures*, **36**, 1996, 131-140
8. Ogin, S.L., Smith, P.A. and Beaumont, P.W.R., *Comp. Sci. Tech.*, **22**, 1985, 23-31
9. Hashin, Z., *Trans. ASME J. Applied Mechanics*, **54**, 1987, 872-879
10. Tsai, C.L., and Daniel, I.M., *Int. J. Solids and Structures*, **29**, 1992, 3251-3267
11. Henaff-Gardin, C., Lafarie-Frenot, M.C., and Gamby, D., *Comp. Structures*, **36**, 1996, 113-130
12. Kashtalyan, M., and Soutis, C., *Adv. Comp. Letters*, **8**, 1999, 149-156
13. Zhang, J., Fan, J., and Soutis, C., *Composites*, **23**, 1992, 291-298
14. Kashtalyan, M., and Soutis, C., *Composites Part A*, **31**, 2000, 107-118
15. Kashtalyan, M, and Soutis, C., *Composites Part A*, **31**, 2000, 335-351
16. Kashtalyan, M and Soutis, C. *Journal of Materials Science*, **41**(20), 2006, 6789-6800.
17. Kashtalyan, M and Soutis, C. *Composites A*, **38**(4), 2007, 1262-1269.
18. Diamanti, K., Soutis, C. and Hodgkinson, J. M. *Composites A*, **36**(2), (2005), 189-195.
19. Diamanti, K., Soutis, C. and Hodgkinson, J. M. *Composites Science & Technology*, **65**(13), (2005), 2059-2067.
20. Diamanti, K., Soutis, C. and Hodgkinson, J. M. *Composites A*, **38**(4), (2007), 1121-1130.
21. Qiu, Z-X., Yao, X-T., Yuan, J. and Soutis, C. *Smart Materials & Structures*, **15**(4), (2006), 1047-1053.